Theoretical study of negative optical mode splitting in LaAlO_{3}

Kurt D. Fredrickson, Chungwei Lin, Stefan Zollner, and Alexander A. Demkov

Phys. Rev. B **93**, 134301 — Published 1 April 2016

DOI: 10.1103/PhysRevB.93.134301

Theoretical study of negative optical mode splitting in $LaAlO_3$

Kurt D. Fredrickson[1], Chungwei Lin[1], Stefan Zollner,[2] and Alexander A. Demkov[1*]
[1]Department of Physics, The University of Texas at Austin, Austin, Texas 78712, USA
[2]Department of Physics, New Mexico State University, Las Cruces, New Mexico 88003, USA

Abstract

We analyze the general circumstances that can lead to the negative longitudinal/transverse optical mode splitting (the Lyddane-Sachs-Teller splitting). As a specific example, we consider the optical phonon frequencies of perovskite $LaAlO_3$ computed within the density functional theory, and compare them to prior experimental reports. The experimental results and theoretical calculation convincingly show that one of the optical mode splittings is indeed negative. The specific optical mode in experiment experiencing the negative splitting is consistent with our analysis. As a typical negative splitting is rather small and close to the experimental resolution, our analysis provides a firm theoretical basis for its existence.

I. Introduction

$LaAlO_3$ (LAO) is a distorted polar perovskite with a rhombohedral crystal structure; bulk LAO crystals are usually twinned and can be considered pseudo-cubic.[1] LAO can be viewed as an alternating stack of positively charged LaO and negatively charged AlO_2 planes. LAO/$SrTiO_3$ heterostructures have been intensely studied due to a two-dimensional electron gas found at the interface,[2] and as a candidate for high-k dielectric grown on Si due to its close lattice match.[3–5] Distortions of the perovskite (cubic) structure lead to a rhombohedral structure with space group $R\bar{3}c$ or D_{3d}^6 (space group 167) at room temperature (Figure 1a).[1,6–8] Experimentally, the crystal is shown to have large longitudinal optical/transverse optical (LO/TO) splitting, in one mode larger than 100 cm^{-1}.[1,9] This splitting arises from long-range Coulomb forces and is known as the Lyddane-Sachs-Teller (LST) splitting. These long-wavelength phonons include an additional coupling to macroscopic electric fields that affects the frequency of the LO modes while leaving the TO modes unaffected. There is, however, interesting experimental work showing that in $LaAlO_3$ (LAO) the splitting may be negative.[9]

In general, the LST splitting is well understood, and in most cases is positive, meaning that in a LO/TO pair the frequency of the LO mode is higher than that of the TO mode. Though there is no obvious reason why that should be always the case, reports of a negative splitting in the literature are sparse. Defects in mixed or doped semiconductors

* demkov@physics.utexas.edu

can cause negative splitting when vibrations due to the defects lie between TO and LO modes.[10–15] There are some experimental reports of negative splitting seen in pure materials such as quartz,[16] garnet,[17] $MgAl_2O_4$,[18] and LAO.[9] However, in these reports the negative splitting is small and close to the experimental resolution, and an affirmative statement of its existence is usually avoided.

Following Born & Huang,[19] the motion of the ions can be separated into transverse and longitudinal modes. The transverse mode $\mathbf{w_t}$ has no additional electric field coupled to it, so its frequency is unaltered by the long-range correction ($\mathbf{w_t} \rightarrow \omega_0$). The frequency of $\mathbf{w_l}$ is affected by the macroscopic electric field ($\mathbf{w}_l \rightarrow \sqrt{\frac{\varepsilon_0}{\varepsilon_\infty}}\omega_0$), leading to an LO/TO splitting (a difference of frequencies near the Γ point), where ε_0 is the static dielectric constant and ε_∞ is the high-frequency dielectric constant. See Figure 1b for a simple example with a unit cell containing one positively charged ion and one negatively charged ion. One can easily derive the LST relation,[20] which determines the static dielectric constant of the material:

$$\frac{\varepsilon_0}{\varepsilon_\infty} = \frac{\omega_{LO}^2}{\omega_{TO}^2} \tag{1}$$

For crystals with multiple optical branches, this is modified[21] to become:

$$\frac{\varepsilon_0}{\varepsilon_\infty} = \prod_i \frac{\omega_{i,LO}^2}{\omega_{i,TO}^2} \tag{2}$$

A major concern of ours, is: can the long-range correction cause a negative LO/TO splitting (*i.e.* can the LO mode of a phonon be lower than the corresponding TO mode)? At first glance, this does not seem possible. The effect of an electric field can only increase the frequency of a mode, due to the extra restoring force needed to overcome the electric field. However, as we shall demonstrate, the negative splitting can indeed occur if there are multiple optical branches. Although the effect of the long-range correction on an individual mode is to increase its frequency, the mixing with the other optical modes can *lower* the frequency of the mode, which allows the overall frequency of the mode to decrease.

We use LAO as our test subject, as negative splitting has been seen experimentally, along with the large LO/TO splitting in some of the modes. That, as we shall see, makes the negative splitting possible. We use a combination of theory, density functional theory (DFT) calculations, and experimental evidence to show that the negative splitting is possible, and in fact occurs in rhombohedral LAO. The rest of the paper is organized as follows. We discuss the LO/TO splitting, emphasizing the circumstances under which the LO/TO splitting can be negative, in Sec. II. In Sec. III, we come to a conclusion.

II. Theory

II.1. LO/TO splitting

LO/TO splitting means that the phonon dispersion $\omega_{\text{phonon}}(\mathbf{k})$ in the vicinity of the Γ-point depends on the direction of approach in k-space. The "splitting" means there are finite energy differences for $\omega_{\text{phonon}}(\mathbf{k})$ infinitely close to the Γ-point. Mathematically, it can be expressed as

$$|\omega_{TO}(k) - \omega_{LO}(k)| \sim O(1), \qquad (|k| < \kappa), \tag{3}$$

where κ is an arbitrarily small momentum. This happens because, in a polar material, the LO mode naturally induces charge accumulation (via the divergence of the lattice polarization $\mathbf{P}_{\text{ion}}$) that costs energy due to the long range static Coulomb interaction. The transverse mode, on the other hand, does not accumulate charge and therefore, its energy is not modified by the Coulomb interaction.[22] Usually, the LO mode is higher in energy, and the LO/TO splitting is *positive*. In the following, using the dielectric function and the dynamical matrix, we discuss how the negative LO/TO splitting can happen. In essence, the negative splitting originates from the mode coupling between different optical branches. This picture shall become clearer when describing the splitting using the dynamical matrix (Sec II.3), and Eq.(3) will become explicit when DFT formalism is introduced (Sec. II.4 and Eq.(10)).

II.2. Negative LO/TO splitting from the dielectric function

Within the harmonic approximation, the phonon contribution to the dielectric function can be described by a few independent oscillators:[19,21]

$$\varepsilon(\omega) = \varepsilon_{\infty} + \sum_{j} \frac{A_j^2}{\omega_{TO,j}^2 - (\omega + i\delta_j)^2}. \tag{4}$$

Here ε_∞ is the electronic contribution, j includes all optical modes, A_j is the oscillator mode strength, δ_j is the broadening of the jth mode, and we use the convention $\omega_{TO,j} < \omega_{TO,j+1}$. The TO and LO frequencies are defined by the poles (maxima) and zeroes of ε in the complex ω plane, respectively.[23] The quantity δ_j is the broadening of the j-th TO mode.

As the poles and zeroes of Eq. (4) occur alternately as ω increases (from zero), the analytic structure (i.e. poles and zeros) of Eq. (4) demands that the LO and TO modes are alternate in energy order, with the lowest energy being that of the TO mode. The positive and negative LO/TO splitting correspond to two different situations, which is best illustrated by considering the limiting cases. On the one hand, when $A_j \ll \omega_{TO,j+1} - \omega_{TO,j}$, the jth LO mode is slightly above jth TO mode in energy, i.e. $\omega_{LO,j} \gtrsim \omega_{TO,j}$, this corresponds to the positive splitting of jth mode. On the other hand, when $A_j \gg \omega_{TO,j+1} - \omega_{TO,j}$, the jth LO mode becomes very close to (j+1)th TO mode, i.e. $\omega_{LO,j} \lesssim \omega_{TO,j+1}$, and this corresponds to the negative splitting of (j+1)th mode. We shall see shortly how this is manifested in a DFT calculation. We would like to mention that whether the LO/TO splitting is positive or negative is determined solely by analyzing Eq.(4) and seeing if $\omega_{LO,j}$ is closer to either $\omega_{TO,j}$ or $\omega_{TO,j+1}$, without any information related to the mode symmetries. In DFT calculations (Sec II.3 and II.4), the symmetry of phonon modes naturally enters the problem, and justifies the discussion here.

To conclude, we would like to make a connection to experiment. Since there are always damping mechanisms leading to a complex dielectric function, Eq.(4) is usually modified to[23,24]

$$\varepsilon(\omega) = \varepsilon_\infty \prod_j \frac{\omega_{LO,j}^2 - (\omega + i\gamma_{LO,j})^2}{\omega_{TO,j}^2 - (\omega + i\gamma_{TO,j})^2} \tag{5}$$

In practice, peaks in Im[ε] and Im[1/ε] are used to identify the TO and LO mode frequencies (poles and zeroes) experimentally. From the peak positions alone, however, one cannot determine how to group the LO/TO modes of the same Γ-point mode. Typically, the LO/TO modes are grouped according to similarity in peak strength and width.

II.3. Negative LO/TO splitting from the dynamical matrix

Theoretically, the phonon dispersion is computed through diagonalizing the dynamical matrix, which can be readily computed within a number of common approximations to DFT. The total dynamical matrix D_{tot} can be divided into two parts

$$D_{tot} = D_{SR} + D_{LR}, \tag{6}$$

where D_{SR} is the short-range component, and D_{LR} is the long-range correction (given in Equation (11)). The details of computing D_{SR} and D_{LR} will be given in the next section. Here we simply note that D_{LR} has only one positive eigenvalue λ_0 and 3N-1 zero eigenvalues; this characteristic eigenvalue λ_0 is constant for a given **k**, and therefore, in its eigenbasis can be written as

$$D_{LR} = \lambda_0 |\alpha\rangle\langle\alpha| \tag{7.1}$$

with $\lambda_0 > 0$ (note that there is no sum over α). In the basis of D_{SR} (labeled by |i>)

$$(D_{LR})_{ij} = \lambda_0 \langle i|\alpha\rangle\langle\alpha|j\rangle = \lambda_0 C_{i\alpha} C_{\alpha j} \tag{7.2}$$

Several properties of D_{LR} should be noted. First, the diagonal components of D_{LR} are always greater than or equal to zero. Second, only modes of non-zero overlap <i|α> couple to one another. We can mathematically *define* the TO (zero <i|α>) and LO mode (non-zero <i|α>) according to its overlap to the state |α>. As the mode coupling is via |α>, only LO modes are allowed to mix together, as the TO modes are never affected by the long-range correction (their diagonal elements are zero). To form the eigenmodes of D_{tot}, all LO modes hybridize due to the long-range correction; though the diagonal term is always positive, it is possible, in some cases, for the overall LO/TO splitting to be negative due to the off-diagonal terms.

To make the origin of the negative splitting more transparent, we consider two LO modes and the consequence of their long-range coupling, with all other optical modes far enough in energy that they do not mix. Without the long-range coupling, the LO 1, labeled as $|1\rangle$, and LO 2, labeled as $|2\rangle$, modes are assumed to have energy Δ and 0 respectively (note that Δ and 0 are also the energies of TO modes, as TO modes are not affected by D_{LR}; also note that 0 here is simply an energy reference, as it is the energy difference that matters). Using Eq. (7.2), we denote $\langle\alpha|1\rangle = y$, and $\langle\alpha|2\rangle = x$, with $x^2 + y^2 < 1$. The total dynamical matrix within these two modes is

$$\begin{bmatrix} \Delta + \lambda_0 y^2 & \lambda_0 xy \\ \lambda_0 xy & 0 + \lambda_0 x^2 \end{bmatrix}, \tag{8.1}$$

whose eigen-energies can be easily found to be

$$E_{LO}^{(1)/(2)} = \frac{1}{2}[\Delta + \lambda_0(x^2+y^2)] \pm \{[\frac{1}{2}[\Delta + \lambda_0(x^2+y^2)]]^2 - \Delta\lambda_0 x^2\}^{1/2}. \quad (8.2)$$

Here the positive/negative sign is for the new LO 1/LO 2 modes, respectively. To preserve the energy ordering of alternating TO and LO modes, the energy of LO 2 has to be between energies of two TO modes, i.e. $0 < E_{LO}^{(2)} < \Delta$. The fact that $0 < E_{LO}^{(2)}$ is obvious from Eq. (8.2), as the second term (the square root) in Eq.(8.2) is smaller than the first term due to the $-\Delta\lambda_0 x^2$. To see that $E_{LO}^{(2)} < \Delta$, we consider

$$\Delta - E_{LO}^{(2)} = \{[\tfrac{1}{2}[\Delta + \lambda_0(x^2+y^2)]]^2 - \Delta\lambda_0 x^2\}^{\frac{1}{2}} - [\tfrac{1}{2}[\Delta + \lambda_0(x^2+y^2)] - \Delta], \quad (8.3)$$

which has to be positive. This can be proved by comparing the square of the two terms in Eq.(8.3), i.e.

$$\{[\tfrac{1}{2}[\Delta + \lambda_0(x^2+y^2)]]^2 - \Delta\lambda_0 x^2\} - [\tfrac{1}{2}[\Delta + \lambda_0(x^2+y^2)] - \Delta]^2 = +\Delta\lambda_0 y^2 > 0.$$

To gain further insight, we now consider three limiting cases. First, we consider $\Delta \gg \lambda_0$, so the long-range term can be treated as a small perturbation. In this case, the energies of LO modes to the leading order in λ_0/Δ are $(\lambda_0 x^2 - \frac{\lambda_0 x^2 y^2}{\Delta})$ and $(\Delta + \lambda_0 y^2 + \frac{\lambda_0 x^2 y^2}{\Delta})$. There is no negative splitting and its energy diagram is given in Figure 2(a). Second, we consider $\lambda_0 > \Delta$, and both x and y are moderate and comparable in values (not vanishingly small). In this case, if one were to neglect the off-diagonal terms, the long-range term pushes the energy of the LO 2 mode higher than that of the TO 1 mode, which appears to contradict our previous discussion that LO and TO modes have to alternate in energy. However, when the off-diagonal terms are taken into account, from Eq. (8.2) we see that the LO 2 mode is pushed down in energy to restore the right energy order. The corresponding energy diagram is given in Figure 2(b). Finally, in Figure 2(c), we consider the case where the long-range correction (no mode mixing) lifts LO 2 above TO 1, and LO 1 is only lifted a small amount, $\lambda_0 y^2 \ll \Delta < \lambda_0 x^2$ in Eq. (8.1). In that case, when $\lambda_0 x^2$ is not too close to Δ, the renormalized LO modes have energies:

$$E_{LO1} = \Delta - \lambda_0 y^2 \frac{\Delta}{\lambda_0 x^2 - \Delta} \quad (9.1)$$

$$E_{LO2} = \lambda_0 x^2 + \lambda_0 y^2 \frac{\lambda_0 x^2}{\lambda_0 x^2 - \Delta} \quad (9.2)$$

We again see that the LO 1 ends up lower in energy than TO 2, and a negative splitting for LO 1/TO 1 occurs. We emphasize that, from Eq. (8.2) and therefore the mathematical constraint of D_{LR}, the energy ordering of alternating TO and LO modes is always preserved. We also note that the middle column in Figure 2 is an "intermediate" step and is only displayed for explanatory purposes. In reality only the last column actually occurs and is the result seen in experiment.

Our analysis thus suggests that when one LO mode "leapfrogs" another in energy, the negative splitting occurs. In a real calculation, which will be presented in the next section, we find that a negative LO/TO splitting indeed happens when two LO modes reverse their energy order after the addition of the long-range correction (See Fig.2c). This is in complete agreement with our previous discussion based on the dielectric function.

II.4. Density Functional Theory

To gain insight into the vibrational spectrum of LAO, we perform theoretical analysis using DFT. First principles calculations are done within the local density approximation (LDA) to DFT using plane augmented-wave pseudopotentials as included in the VASP code.[25–30] We employ the Perdew-Zunger form of exchange-correlation potential.[31] We use the valence configuration $4f^{1}5s^{2}4p^{6}4s^{2}$ for La, $3p^{1}3s^{2}$ for Al, and $2s^{2}2p^{4}$ for O, along with a 600 eV kinetic energy cutoff. For the Brillouin zone integration we use Monkhorst-Pack[32] k-point meshes of (8×8×8) for bulk LAO and (4×4×4) for the (2×2×2) LAO supercell used to calculate the phonons. The crystal structure of bulk LAO is fully optimized with respect to the ionic positions, lattice constants, lattice angles and cell volume until the forces on all atoms are less than 0.1 meV/Å, and the stress is converged to 0.189 GPa. The energy is converged to 10^{-8} meV/cell. The relaxation is not constrained by symmetry.

Using DFT, we calculate the lattice constant of rhombohedral LAO to be a = 5.289 Å, smaller than the experimentally measured lattice constant of a = 5.365 Å, but in good agreement with previous theoretical calculations; we also calculate the cell angle α to be 60.1º, and the octahedral tilting angle φ about the (111)-axis to be 6.2º, again in good comparison with previous theoretical calculations (Table 1). We also calculate the band gap to be 3.88 eV, which is significantly lower than the experimental value of 5.6 eV[5] (a common issue with LDA calculations). The conduction band minimum is located at the Γ point, but the valence band minimum is almost degenerate, located at the FA point with the Γ point value being lower in energy by only 1 meV.

We also use density functional perturbation theory (DFPT)[33,34] to calculate ε_∞ of LAO to be

$$\begin{bmatrix} 4.78 & 0 & 0 \\ 0 & 4.78 & 0 \\ 0 & 0 & 4.72 \end{bmatrix} \quad (10)$$

which is higher than the measured experimental value of 4.12 but in total agreement with previous theoretical results of 4.78, 4.78 and 4.72.[35] The discrepancy in value of the ε_∞ tensor is due to our calculated band gap being smaller than the experimental value, as DFPT uses the calculated band gap; a smaller gap leads to a larger value of ε_∞. For our calculation, we use an average value of 4.76.

To calculate the phonon frequencies, the force constant matrix is constructed using a (2×2×2) supercell of LAO. We then incrementally displace each atom in the central cell slightly from its initial position, and calculate the forces on all atoms in the system. From these forces, we calculate the Hessian by evaluating the second derivative numerically, using a first-order central derivative method. The dynamical matrix is obtained by a lattice Fourier transformation. The phonon spectrum of the system is computed by diagonalizing the dynamical matrix; the eigenmodes of the system are given in the Supplementary Material.[36] In an ionic system, one must also consider the effect of long-range dipole-dipole interactions that is approximated by adding a long-range correction term that depends on the Born effective charges of the material, given by

$$D_{LR,\alpha\beta}(\mathbf{k},\mu,\nu) = \frac{e^2}{V\varepsilon_0\varepsilon_\infty}\exp\left(\frac{-|\mathbf{k}|^2}{\rho^2}\right)\frac{(\mathbf{k}Z^*(\mu))_\alpha(\mathbf{k}Z^*(\upsilon))_\beta}{|\mathbf{k}|^2} \quad (11)$$

where V is the volume of the unit cell, μ and ν are atomic indices, α and β are Cartesian coordinates, ε_0 is the permittivity of free space, and Z* is the Born effective charge tensor. We calculate Z* for each atom in rhombohedral LAO as listed in Table II. The comparison with previous theory is quite good. Further details on calculating the phonon dispersion can be found in the literature.[19,37,38] The Bilbao crystallographic server was used to identify the phonon modes.[39] As the splitting depends on the direction of **k**, there is a range of splittings that we calculate; we find that the direction parallel with the k_z axis gives the best agreement with experiment. See Table III for our comparisons of all modes with prior theory and experiment and see Table IV for our comparisons of IR-active modes with prior theory and experiment. Discrepancies between the prior theory is due to Abrashev *et al.*[40] using a shell model, and Delugas *et al.*[35] using DFT in the generalized-

gradient approximation (GGA) including an additional self-interaction correction on top of the GGA result. In general, our results are in very good agreement with experiment. Of particular note, however, is the LO/TO splitting of the E_u mode with TO frequency 503.74 cm^{-1}. For this particular mode, we calculate the LO/TO splitting to be *negative*, and its origin was discussed in the previous section; this the exact mode that is seen to have a negative splitting in a prior experiment.[9] We also note that our analysis is consistent with a prior report in quartz,[16] where a negative LO/TO splitting was seen when one of the LO modes jumped above another of a different symmetry. The reason this negative splitting is not seen in the prior theory is due to the long-range correction (Eq.(10)) not being included in Ref. [35], and there not being any switching of modes in Ref. [40], which is required in order to observe the negative splitting. Finally, the results are in good agreement with prior reports of negative splitting in doped semiconductors; these negative splittings occur when the frequency of vibration of the dopant lies between another TO/LO pair.[10–15] This is exactly what our prior theoretical results predicts, and is consistent with prior theoretical and experimental reports.

Here we also comment on the highest E_u mode, which has negative splitting in experiment, but not in the DFT calculation. We see that, if we vary the direction of **k** slightly in the long-range correction matrix, we do indeed get a small negative splitting on the order of 5 cm^{-1}. So although in the chosen direction we get no negative splitting (or any splitting at all), when we vary the direction slightly, a negative splitting is seen. We expect that an experiment will never chose exactly one value of **k** and so some nearby **k** vectors would also be expected to be seen in experiment, leading to the measured splitting. This may be related to the twinning of the crystal, which would allow multiple values of **k** to be chosen depending on the relative orientation of the twinning planes.

III. Conclusion

In conclusion, we analyze the general circumstances that can lead to negative LO/TO splitting. We find that negative splitting can occur when an LO mode leapfrogs another LO/TO pair. As a specific example, we consider the optical phonon frequencies of perovskite $LaAlO_3$ computed within the density functional theory, and compare them to prior experimental reports, in which a negative splitting was observed. The theoretical calculation convincingly shows that one of the optical mode splittings is indeed negative. The specific optical mode experiencing the negative splitting found in experiment is consistent with our theoretical and computational analysis. As a typical negative splitting is rather small and close to the experimental resolution, our analysis provides a firm theoretical basis for its existence.

Acknowledgements:

The work at The University of Texas was supported by the National Science Foundation under Grant No. DMR-1207342, through Scientific Discovery through Advanced Computing (SciDAC) program funded by U.S. Department of Energy, Office of Science, Advanced Scientific Computing Research and Basic Energy Sciences under award number DESC0008877, and Texas Advanced Computing Center. The work at New Mexico State University was supported by the National Science Foundation (DMR-1505172).

References

[1] S. Hayward, F. Morrison, S. Redfern, E. Salje, J. Scott, K. Knight, S. Tarantino, A. Glazer, V. Shuvaeva, P. Daniel, M. Zhang, and M. Carpenter, Phys. Rev. B **72**, 054110 (2005).

[2] A. Ohtomo and H.Y. Hwang, Nature **427**, 423 (2004).

[3] A. Knizhnik, I. Iskandarova, A. Bagatur'yants, B. Potapkin, L. Fonseca, and A. Korkin, Phys. Rev. B **72**, 235329 (2005).

[4] X. Lu, Z. Liu, Y. Wang, Y. Yang, X. Wang, H. Zhou, and B. Nguyen, J. Appl. Phys. **94**, 1229 (2003).

[5] S.-G. Lim, S. Kriventsov, T.N. Jackson, J.H. Haeni, D.G. Schlom, a. M. Balbashov, R. Uecker, P. Reiche, J.L. Freeouf, and G. Lucovsky, J. Appl. Phys. **91**, 4500 (2002).

[6] C. Howard, B. Kennedy, and B. Chakoumakos, J. Phys. Condens. Matter **12**, 349 (2000).

[7] X. Luo and B. Wang, J. Appl. Phys. **104**, 073518 (2008).

[8] J. Scott, Phys. Rev. **183**, 823 (1969).

[9] T. Willett-Gies, E. DeLong, and S. Zollner, Thin Solid Films **571**, 620 (2014).

[10] M.Y. Valakh and A.P. Litvinchuk, Sov. Physics, Solid State **25**, 1597 (1984).

[11] E. Vinogradov, B. Mavrin, N. Novikova, and V. Yakovlev, Phys. Status Solidi **247**, 1480 (2010).

[12] L. Genzel, T.P. Martin, and C.H. Perry, Phys. Status Solidi **62**, 83 (1974).

[13] G.M. Zinger, M.A. Il'in, E.P. Rashevskaya, and A.I. Ryskin, Sov. Physics, Solid State **21**, 1522 (1979).

[14] E. Jahne, Phys. Status Solidi **74**, 275 (1976).

[15] E. Jahne, Phys. Status Solidi **75**, 221 (1976).

[16] J. Scott and S. Porto, Phys. Rev. **161**, 903 (1967).

[17] A.M. Hofmeister and A. Chopelas, Phys. Chem. Miner. **17**, 503 (1991).

[18] A. Chopelas and A. Hofmeister, Phys. Chem. Miner. **18**, 279 (1991).

[19] M. Born and K. Huang, *Dynamical Theory of Crystal Lattices* (Oxford University Press, Oxford, 1962).

[20] R. Lyddane, R. Sachs, and E. Teller, Phys. Rev. **59**, 673 (1941).

[21] W. Cochran and R. Cowley, J. Phys. Chem. Solids **23**, 447 (1962).

[22] The current discussion assumes an infinite speed of light and neglects the polariton effect.

[23] D. Berreman and F. Unterwald, Phys. Rev. **174**, 791 (1968).

[24] R. Lowndes, Phys. Rev. B **1**, 2754 (1970).

[25] G. Kresse and J. Hafner, Phys. Rev. B **47**, 558 (1993).

[26] G. Kresse and J. Hafner, Phys. Rev. B **49**, 14251 (1994).

[27] G. Kresse and D. Joubert, Phys. Rev. B **59**, 1758 (1999).

[28] G. Kresse and J. Furthmüller, Comput. Mater. Sci. **6**, 15 (1996).

[29] G. Kresse and J. Furthmüller, Phys. Rev. B **54**, 11169 (1996).

[30] P.E. Blöchl, Phys. Rev. B **50**, 17953 (1994).

[31] J. Perdew and A. Zunger, Phys. Rev. B **23**, 5048 (1981).

[32] H.J. Monkhorst and J.D. Pack, Phys. Rev. B **13**, 5188 (1976).

[33] M. Gajdoš, K. Hummer, G. Kresse, J. Furthmüller, and F. Bechstedt, Phys. Rev. B **73**, 045112 (2006).

[34] S. Baroni and R. Resta, Phys. Rev. B **33**, 7017 (1986).

[35] P. Delugas, V. Fiorentini, and A. Filippetti, Phys. Rev. B **71**, 134302 (2005).

[36] See Supplementary Material at [URL will be inserted by publisher] for more information on the atomic motion of the eigenmodes.

[37] S. Baroni, S. de Gironcoli, A. Dal Corso, and P. Giannozzi, Rev. Mod. Phys. **73**, 515 (2001).

[38] A. Slepko and A.A. Demkov, Phys. Rev. B **84**, 134108 (2011).

[39] E. Kroumova, M. Aroyo, J. Perez-Mato, A. Kirov, C. Capillas, S. Ivantchev, and H. Wondratschek, Phase Transitions **76**, 155 (2003).

[40] M. Abrashev, A. Litvinchuk, M. Iliev, R. Meng, V. Popov, V. Ivanov, R. Chakalov, and C. Thomsen, Phys. Rev. B **59**, 4146 (1999).

[41] H. Seo and A.A. Demkov, Phys. Rev. B **84**, 045440 (2011).

Tables

Table I. Lattice parameters and band gap of LAO.

	a (Å)	E_g (eV)	α (Degrees)	φ (Degrees)
Theory (This work)	5.29	3.88	60.1	6.2
Theory (LDA)	5.29[a]	3.87[a]	60.1[a]	6.1[a]
Theory (LDA)	5.31[b]	3.3[b]	60.2[c]	6.3[c]

[a]Reference [41]
[b]Reference [3]
[c]Reference [35]

Table II. Born effective charges of LAO (e)

	This work DFT-LDA	Theory[a] DFT-GGA
$Z^*_{xx\text{-}La}$	4.46	4.35
$Z^*_{yy\text{-}La}$	4.46	4.35
$Z^*_{zz\text{-}La}$	4.33	4.40
$Z^*_{xx\text{-}Al}$	2.92	2.99
$Z^*_{yy\text{-}Al}$	2.92	2.99
$Z^*_{zz\text{-}Al}$	2.88	2.90
$^{\dagger}Z^*_{xx\text{-}O}$	-2.49/-2.43	-2.47/-2.42
$^{\dagger}Z^*_{yy\text{-}O}$	-2.49/-2.43	-2.47/-2.42
$Z^*_{zz\text{-}O}$	-2.40	-2.43

[a]Reference [35]

[†]There are two types of O with Z_{xx} and Z_{yy} swapped. The off-diagonal terms are all small in comparison with the on-diagonal terms and are not listed here.

Table III: The energy of optical phonons in cm^{-1} and their comparison with prior theory and experiment. The first listed energy is the TO mode and the second is the LO mode; for the non-IR-active modes the TO mode is listed. The corresponding eigenvectors can be found in the Supplementary Material.

Mode Symmetry	Prior theory[a]	Prior theory[b]	Experiment	Theory (This work)
E_g	34	33	34,[b] 33[c]	23.47
A_{2g}	158	141		144.45
E_g	163	146	152[c]	156.44
A_{1g}	132	129	132,[b] 122[c]	164.26
A_{2u}	213/263	168	188(1)/276.4(2)[d]	172.08/279.51
E_u	220/263	179		190.34/190.34
E_u	270/270	297		298.28/298.28
A_{1u}	299	326		344.69
A_{2u}	366/496	409	427.0(1)/596.1(7)[d]	423.96/581.44
E_u	371/475	411		429.69/429.69
A_{2g}	456	458		454.72
E_g	463	454	470[b]	471.93
E_g	691	467	487[c]	503.74
E_u	481/505	478	495.72(1)/495.5(3)[d]	503.74/503.22
A_{1u}	480	480		505.30
A_{2u}	706/712	627	650.79(5)/744.1(9)[d]	671.13/768.13
E_u	707/712	637	708.2(9)/702.2(9)[d]	681.56/681.56
A_{2g}	742	741		780.64

[a]Reference [40]
[b]Reference [35]. Only the TO mode is listed as long-range correction was not included. The paper mistakenly labeled the A_{1u} modes as A_{2g}.
[c]Reference [8]
[d]Reference [9]

Table IV: The energy of the IR-active phonons in cm^{-1} and their comparison with experiment and prior theory. The first listed energy is the TO mode and the second is the LO mode. The second to last E_u modes have negative splitting in agreement with experiment, where the LO mode is lower in energy than the TO mode.

Mode Symmetry	Theory[a]	Theory (This work)	Experiment[b]
A_{2u}	213/263	172.08/279.51	188(1)/276.4(2)
E_u	220/263	190.34/190.34	Not Seen
E_u	270/270	298.28/298.28	Not seen
A_{2u}	366/496	423.96/581.44	427.0(1)/596.1(7)
E_u	371/475	429.69/429.69	Not seen
E_u	481/505	503.74/503.22	495.72(1)/495.5(3)
A_{2u}	706/712	671.13/768.13	650.79(5)/744.1(9)
E_u	707/712	681.56/681.56	708.2(9)/702.2(9)

[a]Reference [40]
[b]Reference [9]

Figure captions

Figure 1. a) The LAO rhombohedral unit cell. The La atoms are green, the Al atoms are blue, and the O atoms are red. The atom numbers correspond to the listed normal modes in Table A1. b) A simple example of LO/TO splitting, for a unit cell with one positively charged ion and one negatively charged ion. Once a specific direction of propagation in momentum space **q** is chosen, phonons can be classified as either TO or LO modes. For a TO mode, the propagating direction is perpendicular to the ionic displacements; for an LO mode, the propagating direction is parallel to the ionic displacements.

Figure 2. The illustration of how the long-range dynamical matrix modifies the phonon energies, involving the energy shift (first-order perturbation) and mode mixing (second-order perturbation). The middle column shows the energy diagram including only the first-order perturbation without the mode mixing. For two energy-wise adjacent LO modes, three possible energy order are presented. a) When the long-range dynamical matrix is weak, the energy shifts of both LO modes are small and the mode mixing can be neglected. b) When both LO modes have strong energy shifts, the mode mixing pushes one of the LO modes below the energy of TO1. c) When the energy shift of the lower LO (LO 2) mode is strong and that of the higher LO (LO 1) mode is weak, then the mode mixing results in a negative splitting. Note that in all three cases, the resulting LO, TO modes are alternate in energy.

Figure 1.
a)

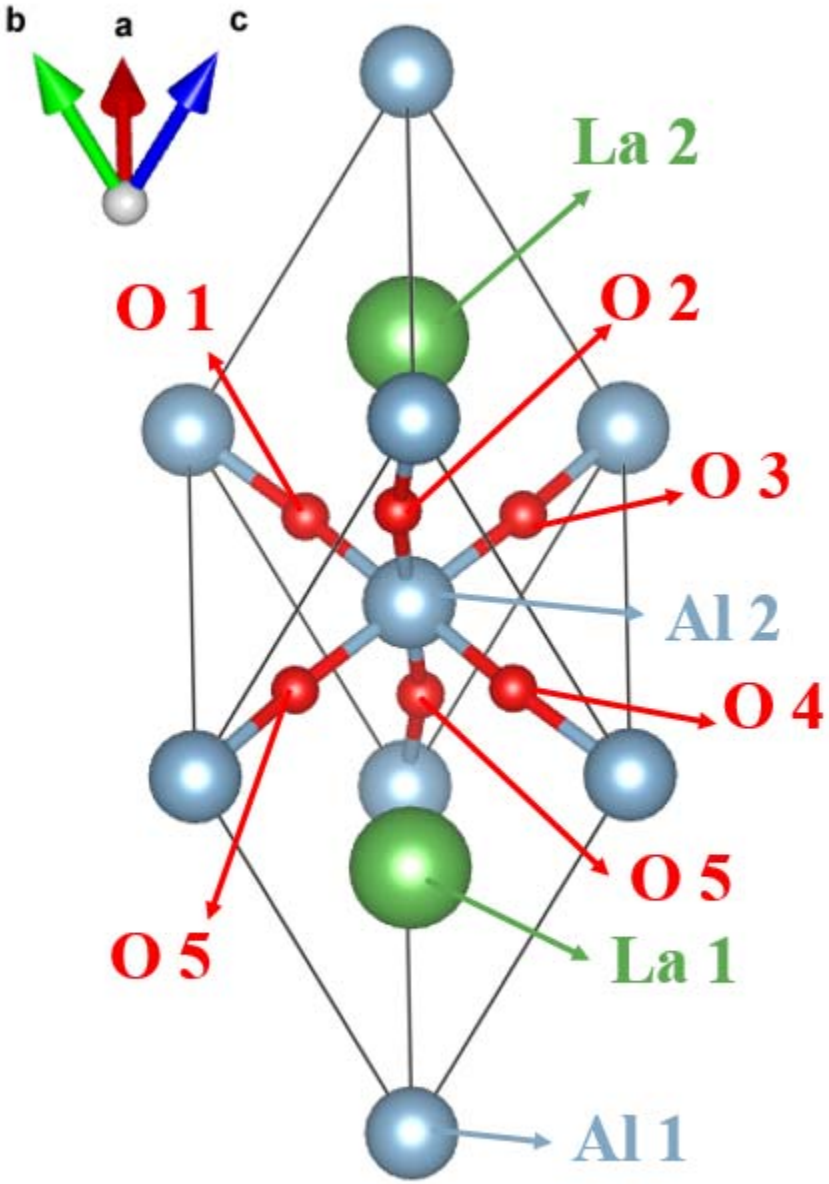

b)

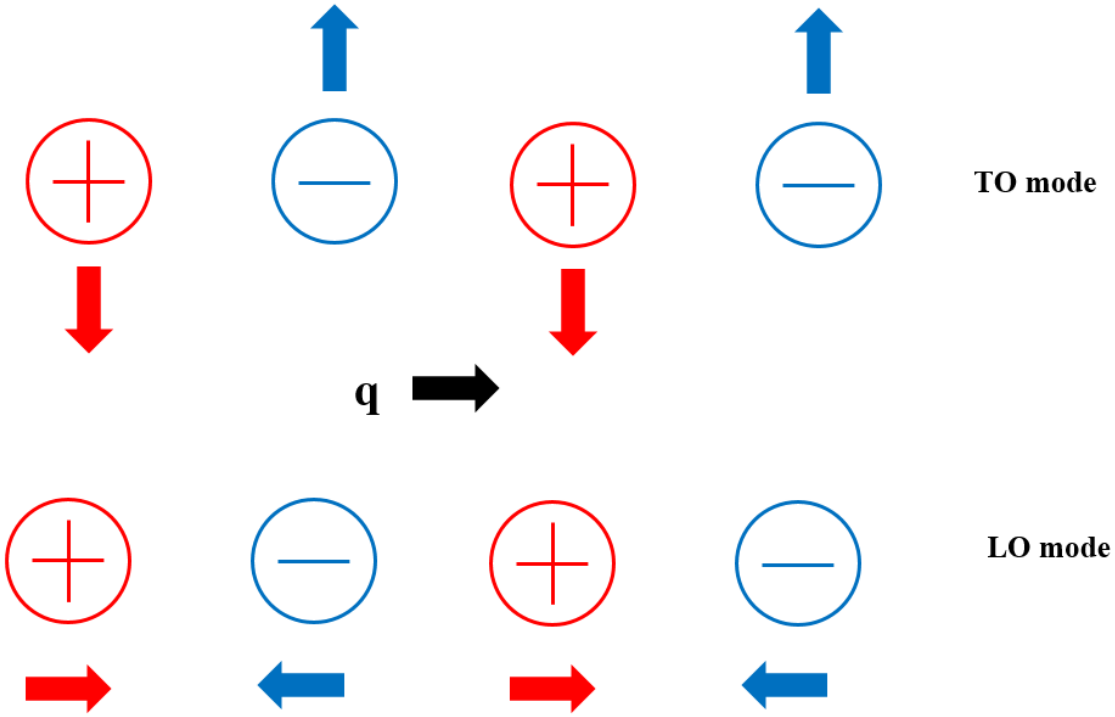

Figure 2.

a)

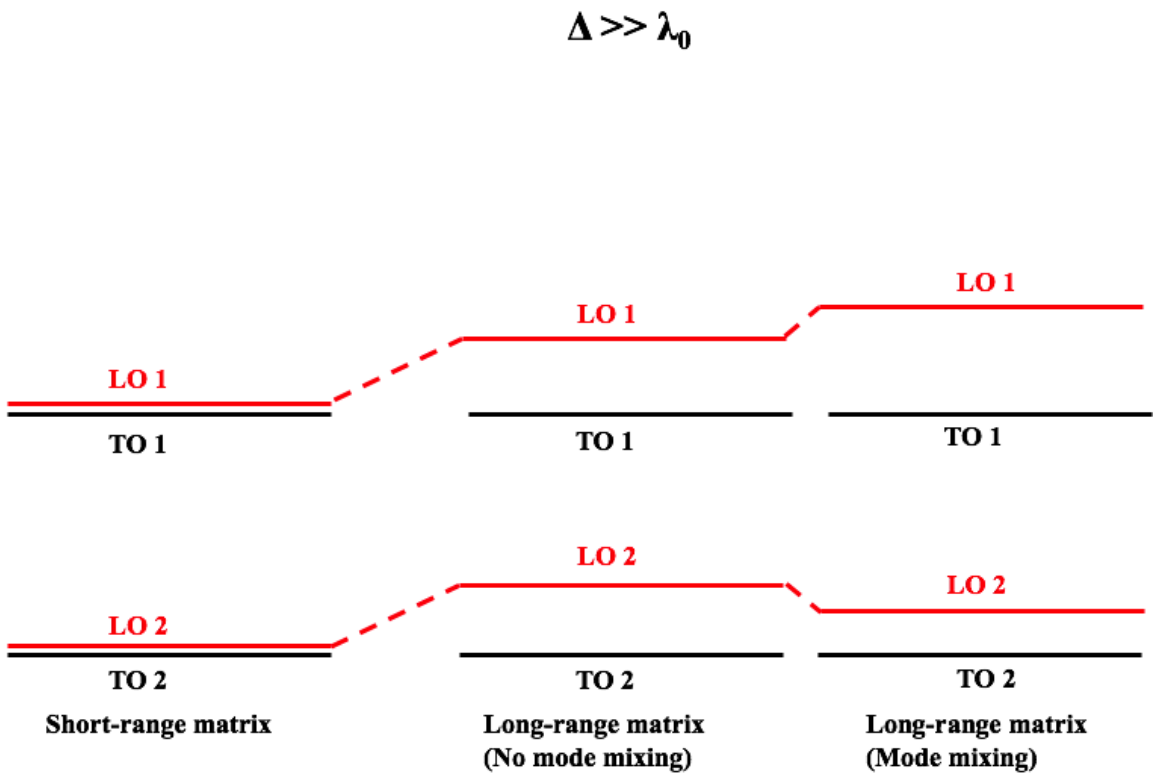
$\Delta >> \lambda_0$
LO 1
TO 1
LO 1
TO 1
LO 1
TO 1
LO 2
TO 2
LO 2
TO 2
LO 2
TO 2
Short-range matrix
Long-range matrix
(No mode mixing)
Long-range matrix
(Mode mixing)

b)

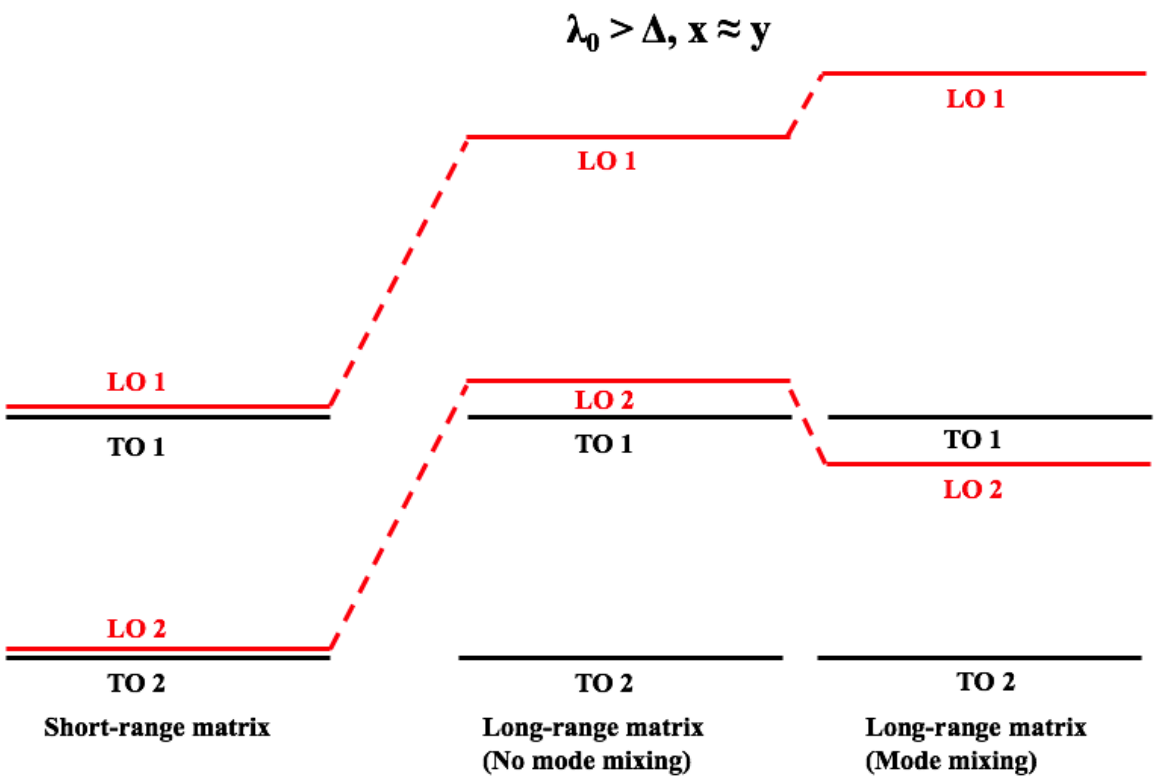
$\lambda_0 > \Delta$, x ≈ y
LO 1
LO 1
LO 1
LO 2
TO 1
LO 2
TO 1
TO 1
LO 2
LO 2
TO 2
TO 2
TO 2
Short-range matrix
Long-range matrix
(No mode mixing)
Long-range matrix
(Mode mixing)

c)

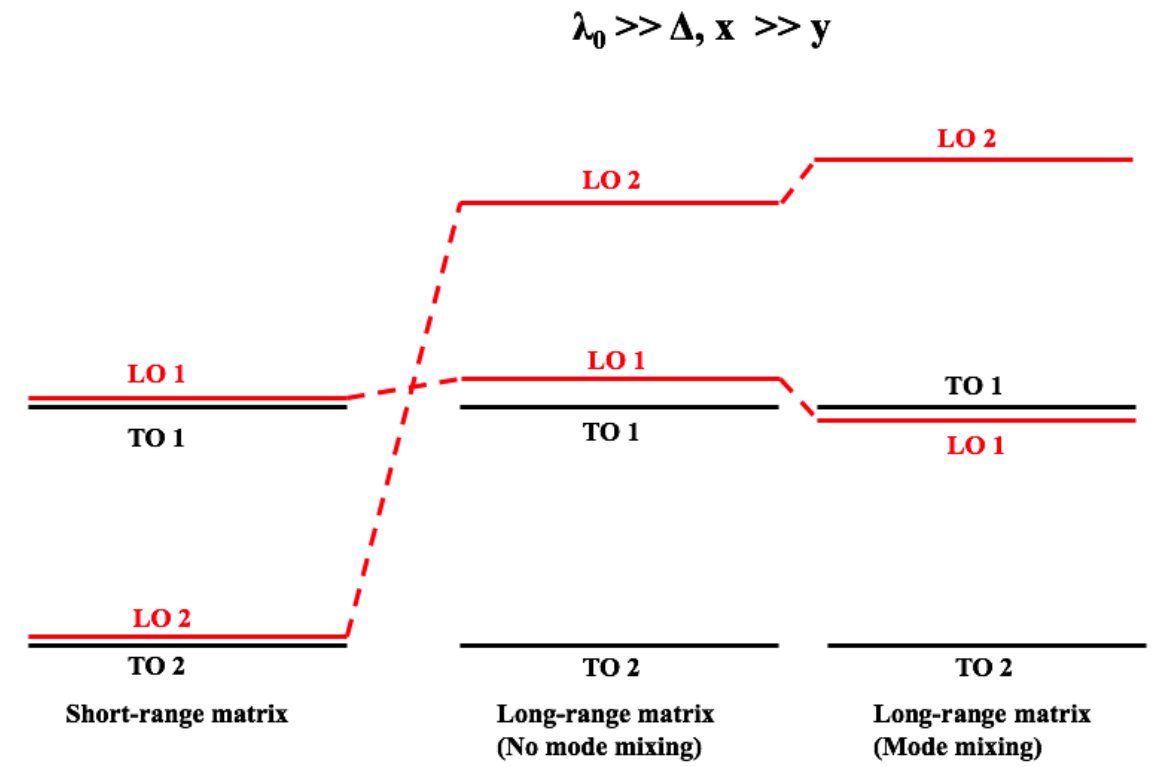
$\lambda_0 >> \Delta$, x >> y
LO 2
LO 2
LO 1
LO 1
TO 1
LO 1
TO 1
TO 1
LO 2
LO 2
TO 2
TO 2
TO 2
Short-range matrix
Long-range matrix
(No mode mixing)
Long-range matrix
(Mode mixing)